Electronic Supplementary Material (ESI) for Physical Chemistry Chemical Physics.

Supplementary Information for

A density functional theory study of the carbon-coating effects on lithium iron borate battery electrodes

Simon Loftager
Juan María García-Lastra
Tejs Vegge*

Department of Energy Conversion and Storage,
Technical University of Denmark,
Fysikvej, 2800 Kgs. Lyngby, Denmark

*Corresponding author: teve@dtu.dk

S1. Parallel graphene coating on $FeBO_3$/$LiFeBO_3$ electrodes

In order to verify that the separation between the electrode surface and the graphene coating is large, as predicted by the PBE+*U* functional, BEEF-vdW+*U* calculations were performed and the results are shown in Fig. 1. As seen, the BEEF-vdW+*U* functional (a) binds the graphene coating to the electrode surfaces with a coating–electrode separation of 3.7 Å, whereas the PBE+*U* functional (b) does not have a local energy minimum. However, the energy is constant for separations of about 4.0 Å and above, indicating a negligible interaction between the coating and the electrode surfaces, and this distance was therefore taken as the optimal coating–electrode distance predicted by the PBE+*U* functional.

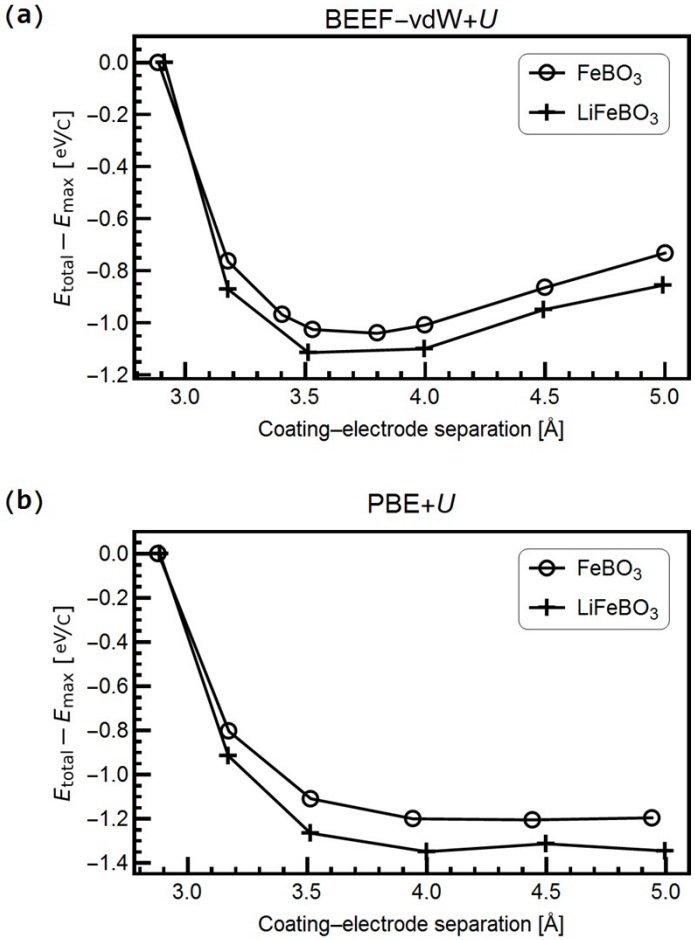

Fig. S1 (a) BEEF-vdW+*U* and (b) PBE+*U* total energies (shifted by the maximum energy).

S2. Stability analysis of $LiFeBO_3$ surfaces

All the surfaces formed in this study maintained the B–O bonds in the borate groups, since breaking these B–O bonds would result in prohibitively large surface energies.

After the cleaving of the (100) surface of the $LiFeBO_3$ electrode, one O atom from two of the BO_3 groups (O atoms A and B in Fig. S2(a)) at this surface protruded outwards from the surface as seen in Fig. S2(a). However, upon relaxation of this surface, a significant tilting of these two BO_3 groups at the surface was observed, as the surface-protruding O atoms moved towards the surface layer to ensure a fourfold O coordination of Li in the surface as seen in Fig. S2(b).

The $LiFeBO_3$ surface energies are calculated by subtracting the energy cost of forming a six-layer slab with the energy cost of forming the same number of layers from the bulk structure. For the (100) surface, the slab in our model—shown in Fig. S2(b)—consists of six layers (one such layer is indicated by the blue box), and a unit cell, consisting of two layers, was used as the bulk structure. Therefore, the surface energy was

$$E_{surf} = \frac{E_{slab}^{six\ layers} - 3E_{bulk}^{two\ layers}}{2A},$$

where A is the (100) surface area of the simulation cell. The very same holds for the (010) surface, where the slab—shown in Fig. 1(c)—also consists of six layers (layer in blue box).

Similarly, for the (001) surface, a six-layer slab—shown in Fig. 2(d)—was used, but along the *c*-axis the unit cell has four layers, and the surface-energy expression for the (001) is therefore

$$E_{surf} = \frac{E_{slab}^{six\ layers} - \frac{3}{2}E_{bulk}^{four\ layers\ in\ c}}{2A}.$$

For all surfaces, the two middle layers of the slab were spatially fixed to the bulk configuration.

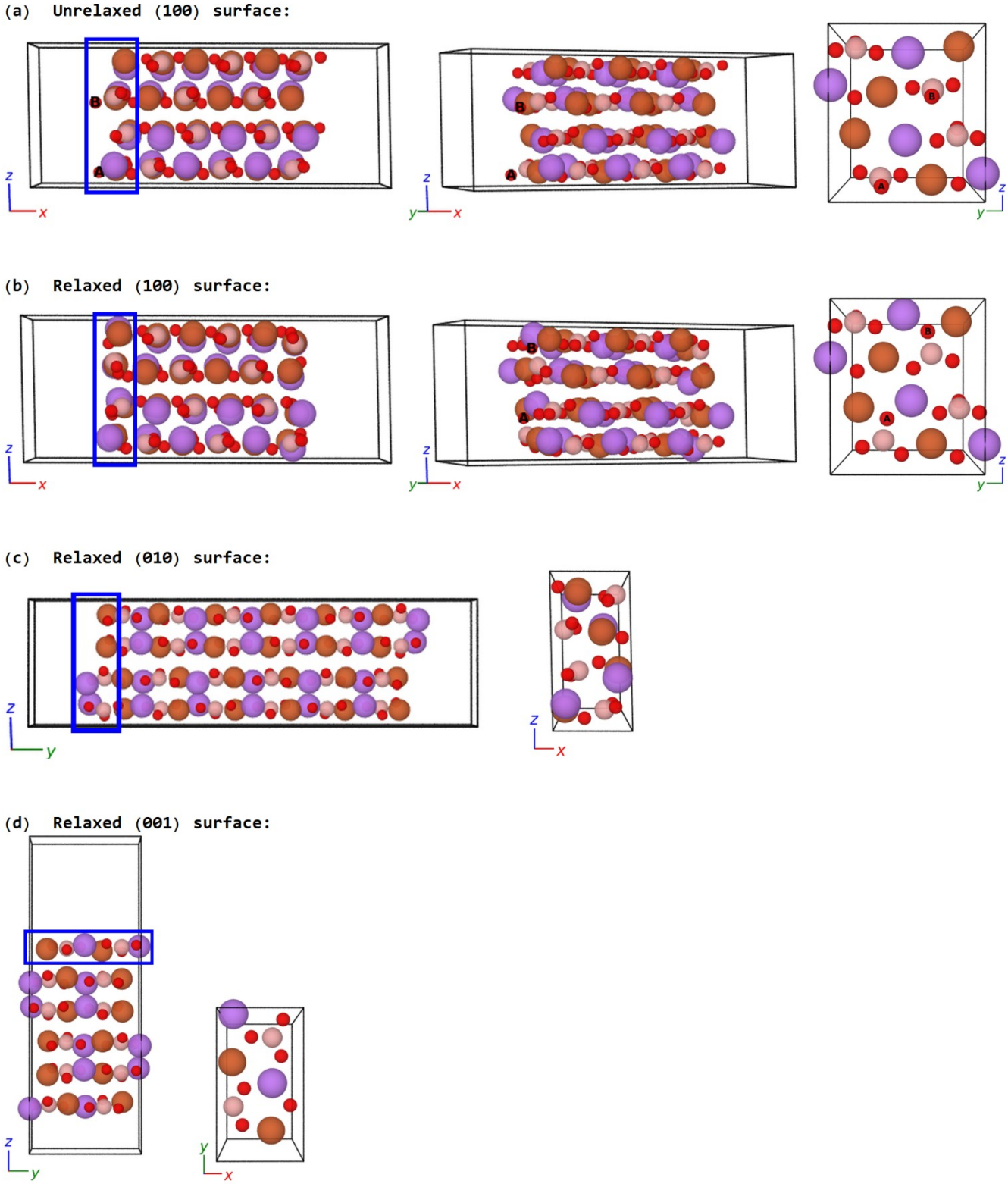

Fig. S2 (a) The (100) surface before structure relaxation, (b) the relaxed (100) surface, (c) the relaxed (010) surface and (d) the relaxed (001) surface of $LiFeBO_3$.

S3. Adsorption of Li ion on pristine graphene

The energy of a Li ion versus the distance to the graphene sheet (coating) is shown in Fig. S3. For these and the below calculations (S3 and S4) on pristine and defected graphene, the same computational method as in the main text was used with the exception of the following details deployed specifically in the graphene study: A $3\sqrt{3}a_1 \times 3\sqrt{3}a_2$ cell was used, sampled on a 2×2×1 *k*-point mesh in the Brillouin zone using a 10 meV Gaussian smearing of the electronic levels.

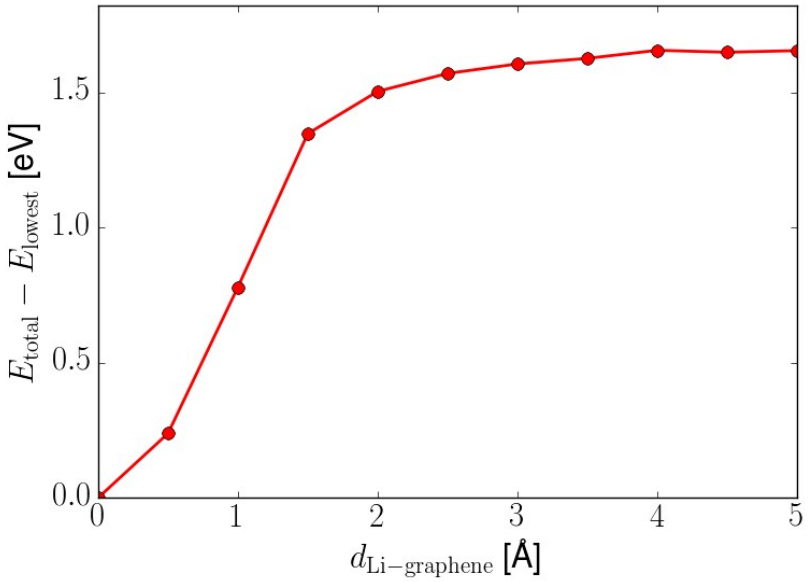

Fig. S3 Energy profile for the adsorption of a Li ion on a pristine graphene sheet as a function of the distance to the graphene sheet.

S4. Activation barriers for Li-ion diffusion through pristine and defected graphene

The activation barriers for Li diffusion through pristine graphene, a Stone–Wales defect, a monovacancy and a 5-8-5 divacancy are shown in Fig. S4. The Stone–Wales defect was formed by rotating two adjacent atoms in the graphene sheet by 90° as shown in the inset in Fig. S4(b). The monovacancy and 5-8-5 divacancy were formed by the removal of one and two atoms, respectively, in the graphene sheet. All the systems remained planar during Li-ion diffusion.

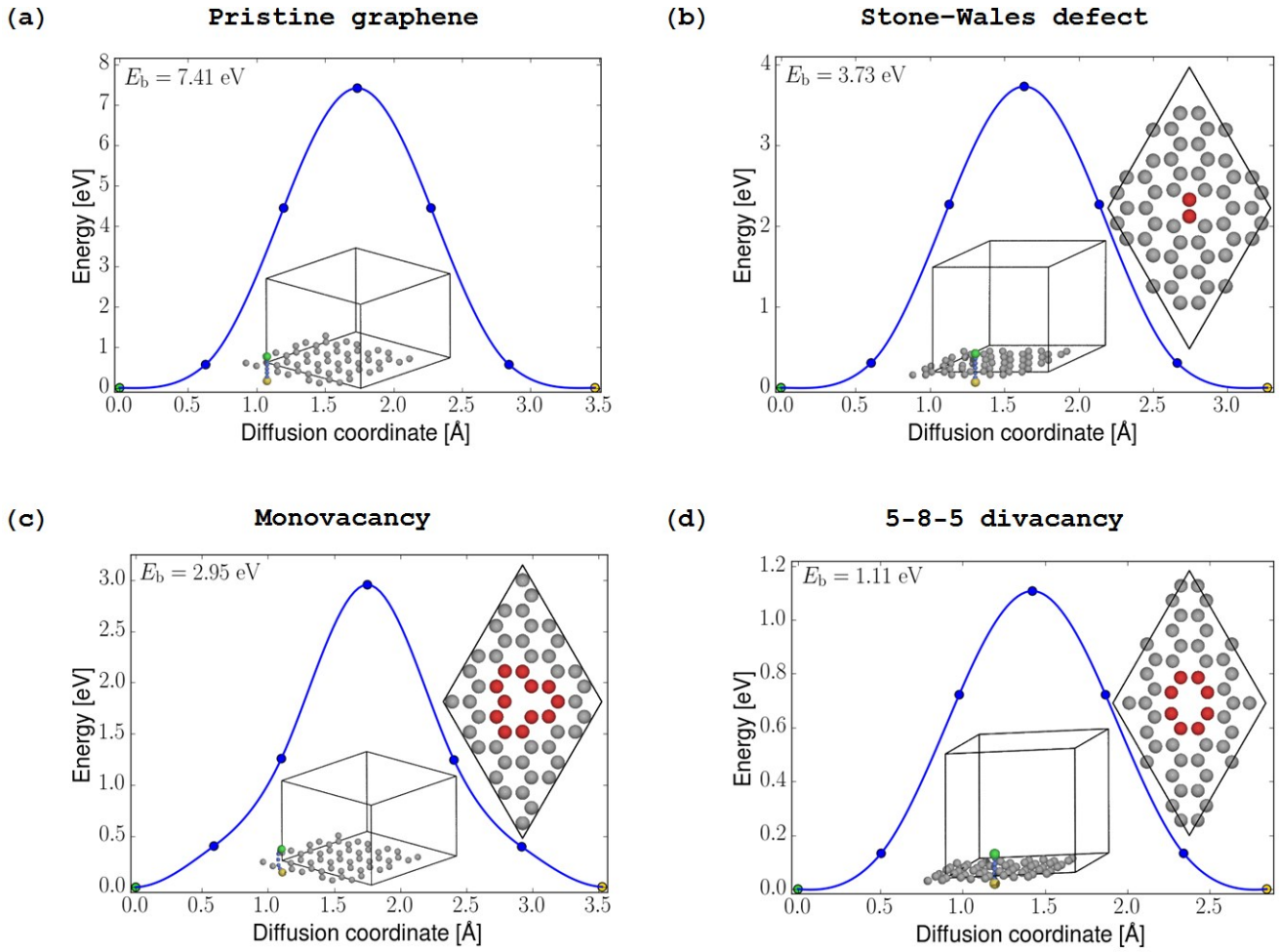

Fig. S4 NEB barriers for Li-ion diffusion through (a) a hollow site of pristine graphene, (b) a Stone–Wales defect with the two C atoms rotated to form the defect shown in red, (c) a monovacancy in graphene with the C atoms surrounding the monovacancy shown in red, and (d) a 5-8-5 divacancy in graphene with the C atoms surrounding the divacancy shown in red.

A previous study[1] of Li-ion diffusion through pristine graphene sheet and a graphene 5-8-5 divacancy found higher NEB barriers than ours, 10.07 and 1.43 eV respectively. It should be noted that the authors in their study used the molecule circumcoronene ($C_{54}H_{18}$) to model graphene. Due to its large HOMO–LUMO gap[2] circumcoronene screens Coulombic interactions poorly as compared to graphene which is a semimetal. This is most likely the origin of the higher barriers calculated in their study. Another study[3] found a NEB barrier of 7.98 eV for Li-vacancy diffusion through graphite which is in good agree with our barrier of 7.41 eV, although the Li concentrations are different, but we do not expect this to significantly affect the diffusion barriers.

S5. Stability of possible anchoring configurations of coating on electrode surfaces

The second-lowest and third-lowest anchoring configurations of the graphene-coating layers to the electrodes are shown in Fig. S5. The energy of the anchoring relative to the B–O anchoring (lowest; discussed in the main text) and bond lengths between coating-edge C atoms and electrode-surface atoms are listed in Tab. S1.

$E - E_{\text{B–O anchoring}}$ [meV / surface-bonding C]	Fe-O anchoring		Fe-B anchoring	
$FeBO_3$	284		1501	
$LiFeBO_3$	470		922	
Bond length [Å]	**Fe–C**	**O–C**	**Fe–C**	**B–C**
$FeBO_3$	2.16	1.33	2.06	1.65
$LiFeBO_3$	2.11	1.39	2.13	1.64

Tab. S1 Energies of the second- and third-lowest configurations relative to the most stable configuration (B–O anchoring) and the bond lengths between the species participating in the anchoring of the coating to the electrode.

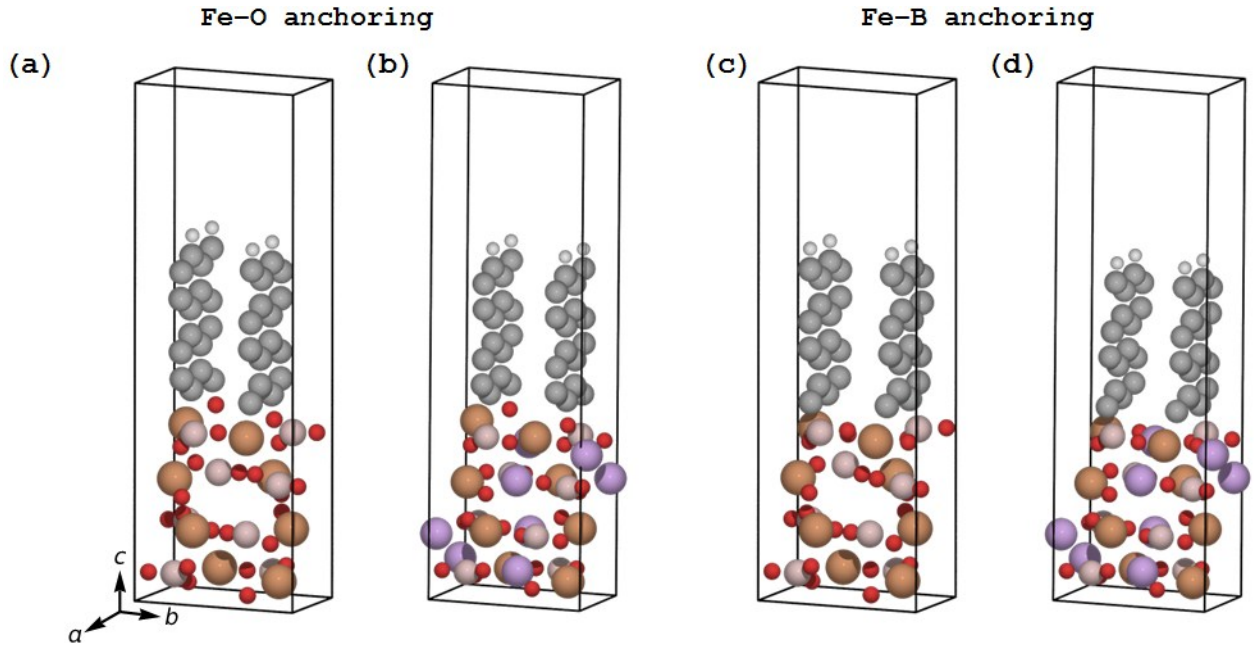

Fig. S5 Anchoring configurations of the graphene coating in which the two C atoms in each coating layer closest to the electrode surface bond (a) to one surface Fe atom and one surface O atom in $FeBO_3$ and (b) $LiFeBO_3$, and (c) to one surface Fe atom and one surface B atom in $FeBO_3$ and (d) $LiFeBO_3$.

S6. Diffusion of Li ions and degradative species in graphite coating

The diffusion barriers for a Li ion moving between two hollow sites in graphite is shown in Fig. S6(a) with a barrier of 0.47 eV. Additionally, we have modeled the diffusion of possible degradative species, H_2O and O_2, in the graphite coating (i.e., graphite far away from the anchoring sites of the misaligned coating on the $FeBO_3$/$LiFeBO_3$ surfaces). The resulting diffusion barrier obtained from a NEB calculation is shown in Fig. S6 with barriers of 1.0 eV for O_2 and 0.1 eV for H_2O diffusion. In all these calculations, the experimental graphite-layer distance of 3.39 Å was used[3].

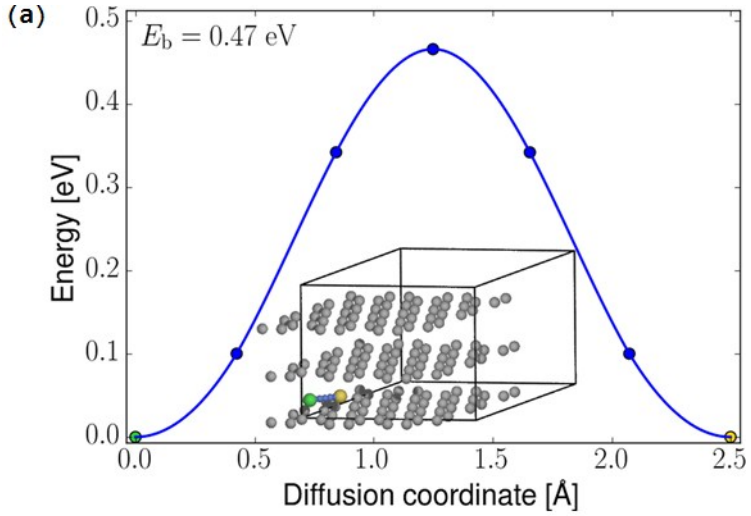
(a)
$E_b = 0.47$ eV
Energy [eV]
Diffusion coordinate [Å]

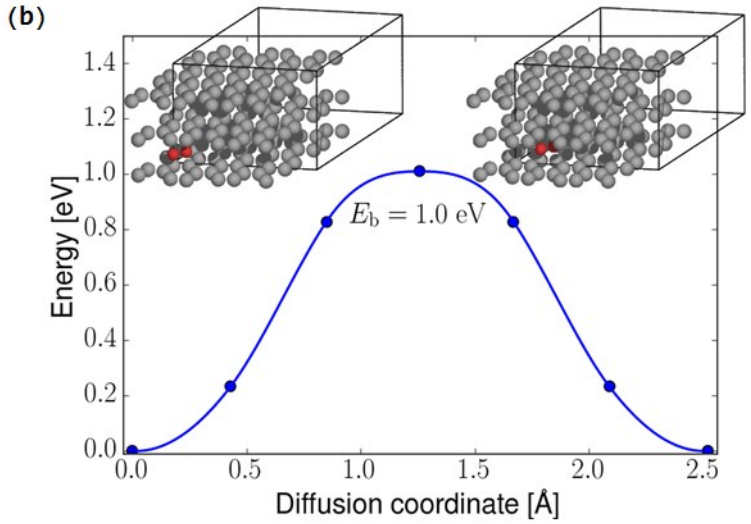
(b)
$E_b = 1.0$ eV
Energy [eV]
Diffusion coordinate [Å]

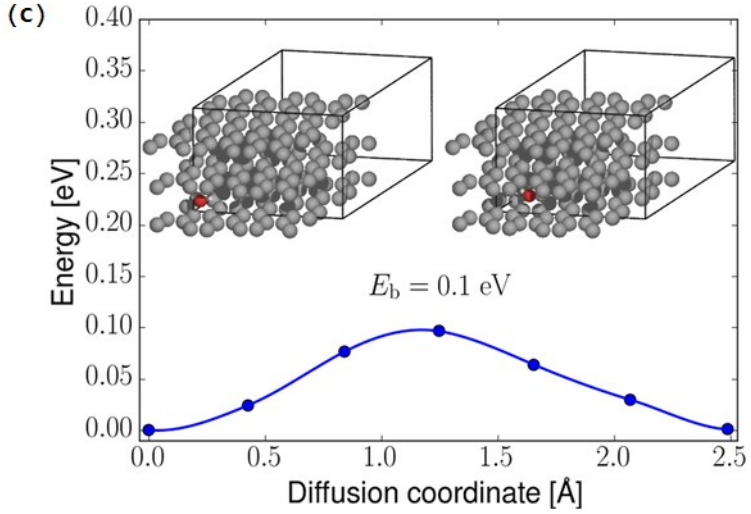
(c)
$E_b = 0.1$ eV
Energy [eV]
Diffusion coordinate [Å]

Fig. S6 NEB-calculated diffusion barrier for species jumping between two adjacent hollow sites in graphite: (a) Diffusion barrier for a Li ion colored in green (initial position), blue (intermediate positions) and yellow (final position). (b) Barrier for O_2 diffusing between two hollow sites with initial (final) configuration shown in the left (right) inset figure. (c) Barrier for H_2O diffusing between two hollow sites with initial (final) configuration shown in the left (right) inset figure.

References

1 D. Das, S. Kim, K.-R. Lee and A. K. Singh, *Phys. Chem. Chem. Phys.*, 2013, **15**, 15128–34.

2 G. Malloci, C. Joblin and G. Mulas, *Astron. Astrophys.*, 2007, **462**, 627–635.

3 S. Thinius, M. M. Islam, P. Heitjans and T. Bredow, *J. Phys. Chem. C*, 2014, **118**, 2273–2280.